PCCP

ROYAL SOCIETY OF CHEMISTRY

PAPER

View Article Online
View Journal

Cite this: DOI: 10.1039/d5cp01295c

Correlation-driven ultrafast charge migration in pyrrole derivatives: the influence of the alkyl group†

Gergely N. Nagy,[ab] Kalyani Chordiya,[cd] Victor Despré,[e] Alexander I. Kuleff[f] and Mousumi Upadhyay Kahaly*[ab]

Received 4th April 2025,
Accepted 7th July 2025

DOI: 10.1039/d5cp01295c

rsc.li/pccp

Pyrrole and its derivatives are essential components of many important organic molecules. By studying their response to ionization, we can gain insights into the photo-assisted reactions they participate in, as well as understand their overall photoresponse. In this study, we examine the effect of alkyl substitution in pyrrole derivatives on the ultrafast charge-migration dynamics initiated by inner-valence ionization. Using a multielectron wave-packet propagation approach, we investigate the correlation-driven charge redistribution in pyrrole (P), *N*-methylpyrrole (MP), and *N*-ethylpyrrole (EP). Additionally, we explore the stability of the π-conjugation structure involving the participation of the nitrogen's lone electron pair. Our findings reveal that as the length of the alkyl chain increases, significant charge migration and charge separation dynamics occur between the pyrrole and the alkyl group with only a small increase in the timescale.

1 Introduction

Pyrrole derivatives are a crucial component of many biomolecules, such as chlorophyll, hemoglobin, myoglobin, cytochrome, or vitamin B12 – which are all naturally occurring metal complexes of the pyrrole molecule. Besides their prevalence in organic molecules,[1,2] they can also play important roles in synthesizing functional materials, such as metal–organic frameworks with high electrocatalytic activity,[3,4] electrochromic copolymers,[5] or highly efficient low band gap photovoltaic materials.[6] Due to the apparent widespread utility of these molecules in both biochemical applications and nanostructures,[7,8] a fundamental understanding of the course of their chemical reactions is crucial. In these, the molecular structure, and correspondingly the structure of the electron cloud, play a fundamental role. An amine substituent can, for example, introduce or change the selectivity of group substitution locations, such as changing the favored location of bonds with metallic centers.[9] In the intrinsically conductive polymeric form of pyrrole, the alkyl group was also found to be influential to the electronic properties of the material, such as charge capacity, solvent transport behavior and ionic resistance.[10] The addition of such groups can introduce or suppress effects such as charge trapping,[11] or lead to increased detector sensitivity, similar to charge trapping through oxygen vacancies in nanophosphors[12] to modulate photoluminescence.

Among the bonds present in pyrrole, the N–H bond is of particular interest due to its proclivity for dissociation and has been widely studied in the literature. UV-photodissociation studies found that the N–H bond of pyrrole is prone to both ground-state and excited-state UV photodissociation with a dissociation energy of 368 kJ mol^{-1}. Furthermore, this dissociation channel is affected by molecular vibrations: an IR + UV excitation resulted in a blue shift of the dissociation peak by 0.23 eV, an enhanced signal, and an increased ratio of the kinetic energy of the fragments to the internal excitations of the resulting pyrroyl radical.[13,14] *Ab initio* results for deuterated pyrrole also point to a significant decrease of the dissociation time in the presence of a pre-excited vibrational state.[15] The type of amine group has also been found to have significant impact on the photoreactivity of the molecule. For example, it is well-established that photoexcitation of pyrrole within the wavelength range of 242 nm to 225 nm leads to fast photodissociation of the N–H bond due to the formation of an excited dissociative πσ* bond,[16,17] while photoexcitation between

[a] ELI ALPS, ELI-HU Non-Profit Ltd, Wolfgang Sandner utca 3, Szeged 6728, Hungary. E-mail: mousumi.upadhyaykahaly@eli-alps.hu
[b] Institute of Physics, University of Szeged, Dóm tér 9, H-6720 Szeged, Hungary
[c] I. Institute for Theoretical Physics and Centre for Free-Electron Laser Science, Universität Hamburg, Luruper Chaussee 149, 22607 Hamburg, Germany
[d] The Hamburg Centre for Ultrafast Imaging (CUI), Luruper Chaussee 149, 22607 Hamburg, Germany
[e] Université Claude Bernard Lyon 1, CNRS, Institut Lumière Matière, UMR5306, F-69100 Villeurbanne, France
[f] Theoretische Chemie, Physikalisch-Chemisches Institut, Universität Heidelberg, Im Neuenheimer Feld 229, Heidelberg D-69120, Germany

† Electronic supplementary information (ESI) available: Additional information is available in the ESI. See DOI: https://doi.org/10.1039/d5cp01295c

250 nm and 240 nm causes a slow tunnel dissociation at the same location.[17] In contrast, in the case of *N*-methylpyrrole, fast (direct) photodissociation happens only with wavelengths above 280 nm, and wavelengths below this only result in slow dissociation mediated by internal conversions.[18]

In this paper, we would like to dive deeper into understanding the charge migration dynamics at the N–H bond in pyrrole and its alkyl derivatives. This study will bring additional information that might help the community to understand the charge migration and charge separation between pyrrole and the N-site substitutes. Although to understand the slow and fast dissociation channels, additional non-adiabatic charge transfer dynamics calculations need to be performed, these calculations are beyond the scope of this study.

Although methylation and ethylation are often categorized as similar alkylation processes, we can see that their influence on the molecular properties can be quite distinct. The molecules considered in our study (pyrrole-G, G = H, CH_3, and C_2H_5) can be separated into two types of groups: the push groups (–G), and the pull group (pyrrole). The kinetics of the charge migration dynamics are expected to change with the size of the push group in our calculations. This will give a detailed understanding of the push–pull mechanism in molecules that naturally occur in biomolecules and in organic/hybrid semiconductors. In this work, we choose to study the charge dynamics resulting from the instantaneous removal of an electron from the molecular systems. Upon such an ionization, a ''hole'', an electron-vacancy is formed in the electron cloud. In cases when the removed electron was in a weak correlation with the rest of the electrons, the hole remains localized, reflecting the molecular orbital of the removed electron. This is usually the case when ionization happens from the outermost valence orbitals. In deeper orbitals, due to the population of states with strong correlation effects, the created hole starts to relocate to other orbitals, beginning a migration throughout the molecule. This is because the ionization of an inner-valence molecular orbital creates a wavepacket by coherently populating several cationic states. This process was considered first in 1999 by Cederbaum and Zobeley[19] and has been termed as correlation-driven charge migration (CM). The process is ultrafast, typically in the few-femtosecond time scale,[20] and in the last two decades, it has attracted a lot of interest, both from the theoretical[20–27] and experimental[28,29] perspective. More recently, it has been considered as a possible enabler for controlling the chemical reactivity of a created ion by influencing the charge distribution within the molecule before the slower nuclear dynamics sets in ref. 29 and 30 – a paradigm known nowadays as ''attochemistry''.

In the following, we will study the dynamics of the charge migration (CMD) driven by electron correlation, with a focus on its sensitivity to molecular structures. Recent findings have highlighted variations in the ultrafast response to ionization in different tautomers of the same molecule.[31] This underscores the importance of understanding how various chemical groups can influence the charge migration process. Such insights could be pivotal in the rational design of molecules with tailored electronic properties that are suitable for performing experimental studies on the phenomenon following the concept of electron-correlation based molecular design.[32–35] Here, we specifically investigate the effect of the alkyl group on the charge migration process in pyrrole (P), *N*-methylpyrrole (MP), and *N*-ethylpyrrole (EP). Utilizing *ab initio* theory, we find that the presence of the alkyl group results in the appearance of an ultrafast charge migration effect upon ionization, and this process is enhanced by increasing the length of the alkyl group.

2 Methods

The equibrillium structures of the neutral molecules are determined using the density functional theory (DFT) geometry optimization routines of the ADF code[36] included in the AMS package.[37–39] For the structural optimizations, we used a QZ4P basis set[40] and the Perdew–Burke–Ernzerhof (PBE) generalized gradient approximation (GGA) functional[41] with no frozen cores and scalar relativistic effects treated *via* the zero-order regular approximation (ZORA). The convergence criteria for the geometry optimization was 2.72×10^{-6} eV for the ground state energy (GSE) and 2.72×10^{-4} eV Å^{-1} for the forces. To allow the utilization of molecular symmetries in the following calculations, the optimized structures were symmetrized with a tolerance of 1% using the SymMol code.[42] An additional optimization executed on the symmetrized structures verified the optimum of the symmetric configuration in all three cases, with the GSE showing a negligible decrease compared to the pre-symmetrization case.

The cationic eigenstates of the studied molecules (noted as $|I\rangle$) were obtained using the non-Dyson algebraic diagrammatic construction scheme at third order (non-Dyson ADC(3)), with the cc-pVDZ basis set. Within this method, the cationic eigenstates are expanded in electronic configurations, which, using the creation and annihilation operators ($\hat{a}_i^\dagger$ and $\hat{a}_i$, respectively), can be written as

$$|I\rangle = \sum_j c_j^{(I)} \hat{a}_j |\Psi_0\rangle + \sum_{r,k<l} c_{rkl}^{(I)} \hat{a}_r^\dagger \hat{a}_k \hat{a}_l |\Psi_0\rangle, \qquad (1)$$

where $|\Psi_0\rangle$ is the correlated neutral ground state of the system, and *j*, *k*, *l* and *r*, *s* are indices of occupied and unoccupied HF orbitals of the neutral ground state, respectively.[43] The first term describes a configuration (referred to as 1h) with only one electron removed from the $|\Psi_0\rangle$ ground state; and the second term represents a configuration (2h1p) where one electron was removed and another was excited onto an unoccupied virtual orbital. At third order, all 2h1p configurations are considered. Going beyond will lead to the incorporation of higher order of excitations (*e.g.* 3h2p configuration), which are necessary when core ionization is considered.[44] Note that the expansion (1) is performed not on the uncorrelated HF ground state, but on the correlated ground state $|\Psi_0\rangle$ obtained *via* Rayleigh–Schrödinger perturbation theory. The ADC(3), therefore, accounts for more correlation than the configuration interaction singles and doubles (CISD) expansion of the cationic state.

The temporal evolution of the system is studied within the framework of sudden ionization. This means that the initial

state of the ionized system is prepared by removing an electron from a HF orbital of its neutral ground state. This approximation considers the ionization to be instantaneous and neglects the interaction between the ionized electron and the created ion. Such ionization can be approximated closely using attosecond pulses with high photon energy. Correspondingly, the temporal evolution of the systems is computed by directly propagating this initial state, using the ADC(3) cationic Hamiltonian and the short-iterative Lanczos algorithm[45,46] in a static nuclei framework. As discussed above, the nuclear response to the disrupted charge density only initiates 5–10 fs after sudden ionization, therefore the neutral geometry of the molecule is considered to be preserved for the propagation. A quantity of particular interest for the description of the CMD is the hole density, $Q(\vec{r}, t)$, as introduced by Cederbaum and Zobeley.[19] This quantity is defined as the difference between the electron density of the neutral ground state ($\rho_0(\vec{r})$) and that of the time-dependent cationic state ($\rho_i(\vec{r}, t)$) after sudden ionization from the φ_i Hartree–Fock orbital:

$$\begin{aligned} Q(\vec{r}, t) &= \langle \Psi_0 | \hat{\rho}(\vec{r}) | \Psi_0 \rangle - \langle \Phi_i(t) | \hat{\rho}(\vec{r}) | \Phi_i(t) \rangle \\ &= \rho_0(\vec{r}) - \rho_i(\vec{r}, t). \end{aligned} \tag{2}$$

In the above equation, $|\Phi_i(t)\rangle$ is the multielectron wave packet of the created ion, and $\hat{\rho}$ is the electron density operator. Using the HF orbitals as a one-particle basis, the hole density can be represented as

$$Q(\vec{r}, t) = \sum_p \left| \tilde{\varphi}_p(\vec{r}, t) \right|^2 \tilde{n}_p(t), \tag{3}$$

where $\varphi_i(\vec{r}, t)$ are referred to as natural charge orbitals (NCOs) and $\tilde{n}_p(t)$ are their hole-occupation numbers. At each time t, the former are different linear combinations of the HF orbitals of the neutral molecule, while the latter indicate how the initially created hole charge is distributed among NCOs at that point of time. For details on the construction of the hole density and its analysis with the help of the NCOs and hole-occupation numbers, the reader is referred to ref. 43 and 47.

3 Results

3.1 Symmetry and ionization spectrum

We start with analyzing the symmetries present in the molecules and their HF orbitals. Following the DFT geometry optimization procedure described in (Section 2), we find that the optimal structure for P has C_{2v} symmetry, with four irreducible representations (irreps) (A_1, B_1, A_2, and B_2). This is lowered to C_s in the case of MP and EP with only two irreps (A' and A''). Hence, this partial symmetry breaking from P to MP can potentially result in increased mixing. The optimized structures, the symmetry elements of their respective symmetry group, and the HF orbitals relevant for the upcoming discussion of the CMD are shown in Fig. 1. The symmetries of the occupied HF orbitals are classified in Table 1 for each molecule by their corresponding irrep of the symmetry group.

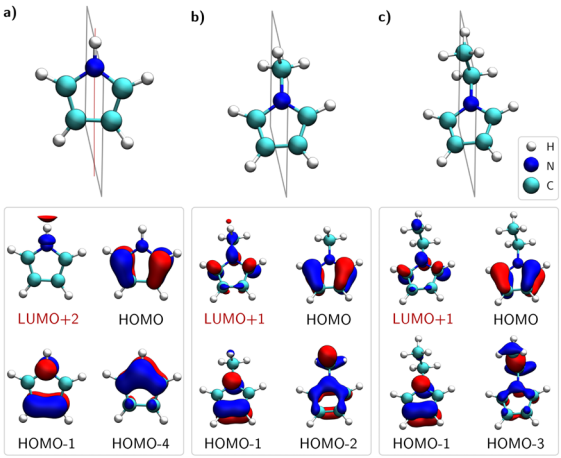

Fig. 1 The structures and selected HF orbitals of (a) P, (b) MP and (c) EP. The symmetry plane of the C_n symmetry group, and the additional 2-fold rotational axis of C_{2v} is also shown. Below each molecule, the HF orbitals which are significantly involved in the charge migration effect are shown, represented by isosurfaces at $\pm 0.075e\ a_0^{-3}$. The complete set of HF orbitals is shown in Fig. S1 (ESI†).

An important aspect governing the hole migration, specifically the appearance of avoided crossings in the hole-population evolution, is the symmetry classification of the involved orbitals. If two or more orbitals reside in the same irreducible representation (irrep), the hole occupation number of their corresponding NCOs cannot become equal, and instead an avoided crossing takes place where the two involved NCO exchange orbital character through a strong mixing of their orbital basis components. Conversely, if two states transform under different irreps, no such mixing takes place and they can cross freely. This can be observed upon the evolution of the hole occupation number, as will be seen later (in Fig. 3).

We start our ADC-based procedure by calculating the ionization spectra of the molecules, which contains the main fingerprints of correlation between the cationic states.[43] These, computed using the nD-ADC(3) method with the cc-pVDZ basis set, are shown in Fig. 2. Each line in the spectra corresponds to a cationic eigenstate of the system, with its height representing the spectral intensity derived from the 1-hole (1h) part of the respective state. Since all states are normalized to 1, the difference between 1 and the spectral intensity of a given state indicates the contribution of its 2-hole-1-particle (2h1p) configurations. This "invisible" part of the stick spectrum therefore reflects the degree of electron correlation in the corresponding state.

The first two ionic states in each molecule are predominantly 1h states, populated by removing electrons from the HOMO and HOMO−1, respectively. The first ionization potentials are 8.18 eV for P, 7.79 eV for MP, and 7.74 eV for EP. These values closely align with the experimental results of 8.2 eV for P[48] and 7.94 eV for MP.[49] The observed redshift in the ionization potentials can be attributed to the donor character of the methyl and ethyl groups in the pyrrole ring.[50] A similar redshift appears in the second ionization potentials, which occur at 9.07 eV for P, 8.38 eV for MP, and 8.31 eV for EP. Interestingly, there is a significant gap of several eV before the next group of states

Table 1 Symmetry classification of the occupied HF orbitals (denoted by i as in HOMO−i; HOMO: i = 0). The orbital whose ionization leads to the significant charge migration effect discussed in this article is marked with a star

	Pyrrole (P)	Methylpyrrole (MP)	Ethylpyrrole (EP)
Sym.	A_1: 2, 6, 7, 9, 11, 12 B_1: 1, 4*	A′: 1, 2*, 3, 6, 8, 9, 10, 12, 14, 15	A′: 1, 3*, 4, 5, 8, 9, 11, 12, 14, 16, 17, 18
Antisym.	A_2: 0 B_2: 3, 5, 8, 10	A″: 0, 4, 5, 7, 11, 13	A″: 0, 2, 6, 7, 10, 13, 15

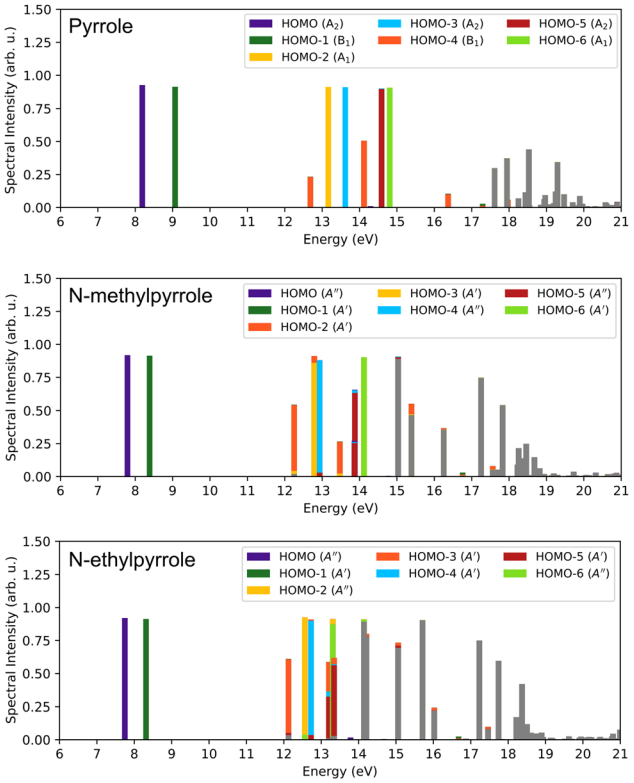

Fig. 2 Ionization spectra of the three examined systems. Orbitals below HOMO−6 are colored with gray. The position of the bars corresponds to the orbital energy of the respective cationic state; the height is determined by the corresponding spectral intensity at these energies; and the colors describe the weight of each one-hole configuration in the respective cationic state.

emerges, which occurs above 12 eV for all molecules. In this region, we observe the appearance of satellite states, which are characterized by a large contribution of 2h1p configurations, reflecting additional excitations that accompany electron removal. In particular, we can observe satellite states with HOMO−4 character in P, featuring a main line at 14.12 eV and two satellites at 12.68 eV and 16.37 eV, as seen in Fig. 2. Similarly, satellite states are present for HOMO−2 in MP, with a main line at 12.25 eV and satellites at 13.48 eV and 15.38 eV. In EP, satellites are observed for HOMO−3, with a main line at 12.12 eV and satellites at 13.21 eV and 13.34 eV (see Fig. 2).

From the Hartree–Fock (HF) analysis (Fig. 1), we can see that the charge-density distribution in these molecular orbitals is similar across P, MP, and EP, and they all belong to the same irrep (B_1 or A′ for P). Heuristically, these orbitals can be described as the continuation of P HOMO−4 as the alkyl group is added or extended. Furthermore, in both MP and EP, these orbitals exhibit significant charge distribution on the alkyl group in a similar manner. This characteristic indicates the dominance of π bonds, which contribute to the in-plane stability of the pyrrole ring[51] and make these orbitals more sensitive to symmetry-disrupting perturbations caused by the methyl or ethyl groups. The π nature of these orbitals also aligns with the presence of significant electron–electron correlation effects. Furthermore, these orbitals bear a resemblance to the orbital responsible for the charge migration dynamics, characterized by long-lived electron coherence, in the benzene molecule.[22] It would be intriguing to investigate in future studies whether this behavior is a signature of delocalized π systems.

When comparing the energy gap between the second cationic state (with HOMO−1 character, green line in Fig. 2) and the satellite/main state in the 2h1p configuration (orange lines in Fig. 2), we observe an increase from 3.61 eV in P to 3.87 eV in MP, with a similar value of 3.81 eV in EP. The first two cationic states result from ionization of molecular orbitals with π character, mainly distributed over the carbon atoms of the pyrrole ring. In contrast, the third cationic state involves charge distribution in orbitals such as HOMO−4 for P, HOMO−2 for MP, and HOMO−3 for EP, which include the nitrogen lone pair participating in the π-conjugation structure. A similar configuration, though with a smaller gap, has been observed in porphyrin.[52] This substantial energy gap, exceeding 3 eV in the lower energy part of the ionization spectrum, allows us to distinguish between the conjugation structures with and without lone-pair electron contributions.

The ionization spectrum becomes increasingly complex beyond 16 eV, with numerous closely spaced 2h1p states forming a quasi-continuum. In this regime, the molecular-orbital picture of ionization breaks down due to strong correlation effects,[53] leading to the formation of the so-called correlation band, a phenomenon seen in ionization from inner-valence orbitals.[54,55] Finally, it is worth noting that the second excited state of each system is either the main state or part of a main-state-and-satellite structure, as discussed earlier, with strong electron correlation effects stemming from one specific orbital. This suggests that the electron correlation structures are stable even as the carbon chain length increases, indicating the possibility of designing molecules based on these stable correlation patterns, as seen in previous studies on systems of systematically increased size.[32,35]

3.2 Charge migration dynamics

In order to examine whether the common features in the ionization spectra lead to similar charge dynamics upon

ionization, we computed the evolution of the hole density (eqn (3)) following the ionization of HOMO−4, HOMO−2, and HOMO−3 of P, EP, and MP, respectively. First, we examine the hole occupation of the NCOs that take on a significant occupation at some point during the charge migration process. The temporal evolution of the hole-occupation numbers $\tilde{n}_p(t)$ of these NCOs in each case is depicted in Fig. 3(a). A positive occupation represents a hole in an occupied orbital, while a negative value describes an electron excited to the respective unoccupied orbital. The color of each occupation number gives the leading component of the HF orbital basis used to expand the natural charge orbitals (see, Section 2). In general, the NCOs consist of a singular dominant member of the HF basis, except near avoided crossings of the occupation number between orbitals of the same irrep, where strong orbital mixing happens due to short-lived electronic coherence, and the NCO changes its HF character. The changes of the line colors on 3 reflect this phenomena.

The energy difference between the main state and the dominant satellite line (ΔE) of the ionized orbital (ΔE_P = 1.44 eV, ΔE_P = 1.23 eV, and ΔE_P = 1.09 eV; see Fig. 2 and related discussion in Section 3.1) defines a characteristic main oscillation period for the charge migration as $T = 2\pi\hbar/\Delta E$.[20] This is T_P = 2.87 fs for P, T_{MP} = 3.36 fs for MP, and T_{EP} = 3.79 fs for EP. The evolution is also shown in terms of the main oscillation period of each molecule. A corresponding phase of this charge-migration oscillation can be defined as $\varphi_{CM} = t/T$. In the following, we will use this quantity to compare the CMD between the three molecules at different phases of the oscillation.

From Fig. 3(a), we can observe that the overall evolution of the hole occupations is quite similar for the three molecules. In less than 2 fs, we observe a significant increase of the hole population on the HOMO, which is antisymmetric and localized almost exclusively on the four carbon atoms of the pyrrole ring, as opposed to the initially ionized orbitals, which are symmetric and are predominantly localized on the N-atom and on the attached alkyl in MP and EP (see Fig. 1). The hole population on HOMOs exceeds 1, showing that in addition to the migration of a substantial fraction of the initial hole there, a simultaneous excitation from the HOMO to LUMO+1 or LUMO+2 takes place. In all three cases, one other orbital obtains significant hole occupation, which corresponds predominantly to HOMO−1. This orbital, which – like HOMO – is mostly unaffected by the alkyl group on the N-site (*cf.* Fig. S1, ESI†), has the same symmetry (belongs to the same irrep) as the initially ionized one, and is localized on the pyrrole ring. The occupation of HOMO−1 and the ionized orbital evolve similarly, and roughly oppositely to the HOMO.

The evolution of the hole density, $Q(\vec{r}, t)$, is visualized in Fig. 3(b) by isosurfaces at selected phases of this oscillation until φ_{CM} = 1.5. At t = 0, the hole distribution is identical to the

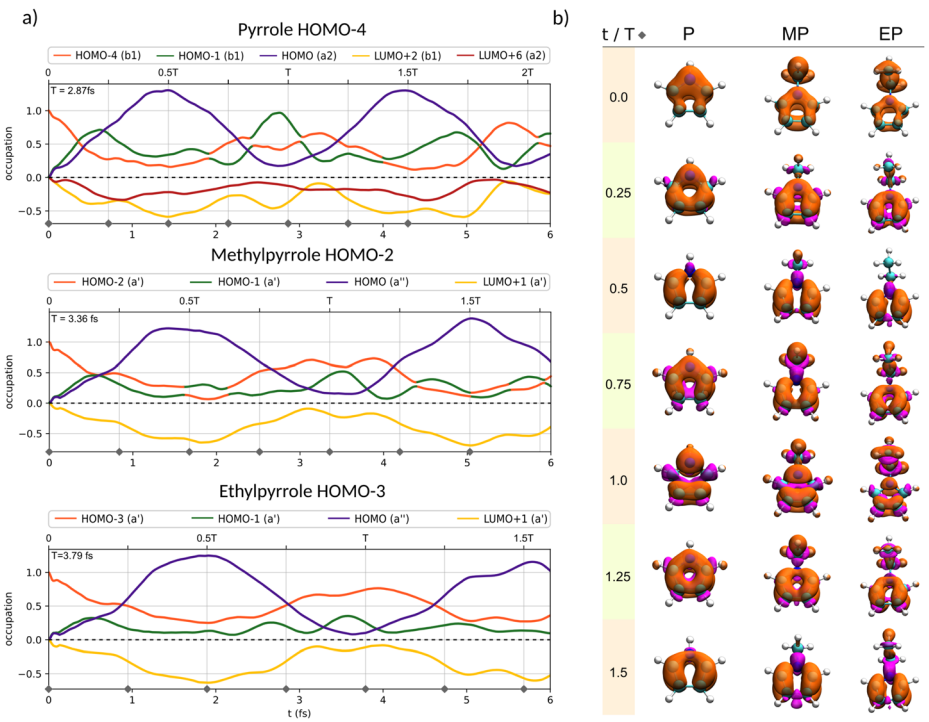

Fig. 3 (a) Hole occupation of the evolving orbitals upon which the change of occupation over time is significant. Each continuous line represents a natural charge orbital, while the colors correspond to the dominant member of its HF orbital basis at the given point of time. Avoided crossings can be observed between NCOs of the same symmetry. The time is shown both in fs and in units of the (molecule-specific) characteristic CM oscillation period T of the respective molecule. (b) Temporal evolution of the hole density after ionization from the respective orbitals at selected phases ($\varphi_{CM} = t/T$) of the main period of each molecule. The isosurface at 0.004 is shown for the hole density (orange) and at −0.001 for the excess electron density (pink). The temporal location of the snapshots is marked in (a) with gray diamonds.

HF orbital from where the electron is removed, corresponding to the initial condition of sudden ionization. As the time proceeds, the distribution relocates to a shape closer to that of the HOMO of the molecule, as the corresponding NCO obtains the largest hole population number around $\varphi_{CM} = 0.5$ This hole distribution is significantly different from the initial one, where the hole is delocalized on the entire molecular backbone. Instead, the hole migrates away from the donor group, G, (where G = H, CH_3, C_2H_5 in P, MP, and EP, respectively): the initiated correlation-driven charge migration dynamics represent a transfer of charge from the π-conjugated carbons of the pyrrole to the donor group of the molecule. We see that in the case of MP and EP, a significant fraction of the charge migrates back-and-forth between the pyrrole ring and the alkyl group, jumping over larger distances with the increase of the chain, but keeping nearly the same timescale. This feature offers interesting possibilities for designing molecules with pronounced charge-migration dynamics in which the charge can be transported fast over large distances.

In addition to the spatial distribution of the hole density, the overall extent of the charge migration between the pyrrole ring and the alkyl group is also of particular interest, as this effect can be directly related to the photodissociation of the alkyl–pyrrole bond. To quantify the amount of charge located on or transferred between these two groups in the molecules, we calculate the hole density along the molecular axis, z (see Fig. 4(a)–(c)), connecting the two groups, and integrate over the remaining two spatial dimensions:

$$\tilde{Q}(z,t) = \iint_{x,y} Q(\vec{r},t)\mathrm{d}x\,\mathrm{d}y. \tag{4}$$

As we are interested in comparing how much charge is donated from the –H in P, $-CH_3$ in MP, and $-C_2H_5$ in EP, we integrate $Q(z,\ t)$ below and above the mid-point between the N–H, N$-CH_3$, and N$-CH_2$ bond in P, MP, and EP, respectively, to obtain the hole density on the pyrroyl ring and on the donor group:

$$\bar{Q}_P(t) = \int_{-\infty}^{z_N} \tilde{Q}(z,t)\mathrm{d}z \text{ and } \bar{Q}_G(t) = \int_{z_N}^{\infty} \tilde{Q}(z,t)\mathrm{d}z. \tag{5}$$

Fig. 4(a)–(c) show the time evolution of $\bar{Q}_P(t)$ and $\bar{Q}_G(t)$ for the three molecules. We can observe that initially, the charge density is distributed both on the pyrrole ring and the donor groups. Around halfway through the CM oscillation ($\varphi_{CM} = 0.5$), most of the hole density gets relocated to the pyrrole ring, leaving almost no hole occupation on the donor group. The process is then reversed and the charge migrates back to the donor group. We can observe that as the length of the alkyl group increases, the extent of charge migration between the alkyl group and the pyrrole ring also increases, together with a slight increase in the characteristic duration of the CM oscillation (the second peak is reached at 4.0 fs, 4.8 fs, and 5.3 fs for P, MP, and EP, respectively). In the case

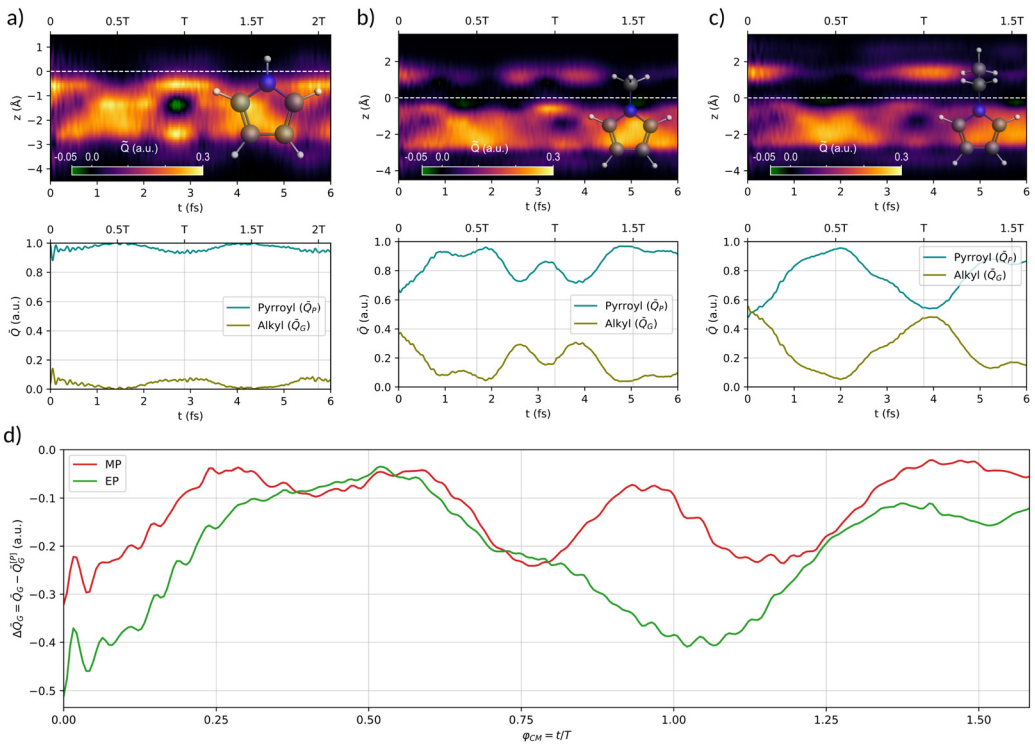

Fig. 4 (a)–(c) The charge density of (a) pyrrole, (b) MP, and (c) EP integrated in the planes perpendicular to the molecular axis (top), and integrated in the volume containing the pyrrole ring and in the volume containing the *N*-substituent (bottom). The volume is split at the midpoint of the N–H or N–C bond by a plane perpendicular to the molecular axis (marked by a dashed white line). (d) Excess charge relative to pyrrole (marking the relative deficiency of hole density) located on the pyrrole ring ($z < 0$ on (a)–(c)) at certain periods of the oscillation. The difference is taken at given fractions of the main oscillation period T of each molecule.

of P, we can observe a clear charge oscillation between the pyrrole ring and the hydrogen atoms. This is similar to the oscillation observed for the charge migration in benzene.[22] However, in P due to the electron-withdrawing nitrogen, the hole density located on the hydrogens attached to C–N–C part of the pyrrole ring is higher compared to the other two hydrogens on the lower part of the chain (see hole density on P at $\varphi_{CM} = 0.75$ and $\varphi_{CM} = 1.25$ in Fig. 3(b)). In the case of MP, we can also observe a second mid-peak between the two main peaks at $t = 3.2$ fs, causing a bounce-back of the hole density. This effect is explained by the strong second satellite at 15.38 eV, which introduces a secondary oscillation with a characteristic period of 1.32 fs. In EP, this effect is much weaker as the similar satellite at 15.05 eV has much less contribution from the ionized orbital while also exhibiting weaker correlation. Consequently, we can observe a significantly amplified variation in the hole density evolution: the initial charge density is almost evenly distributed between the ring and the ethyl group (with an initial integrated charge density of $\bar{Q}_G(t = 0) = 0.56e$ on the group, compared to $\bar{Q}_G(t = 0) = 0.07e$ in P and $\bar{Q}_G(t = 0) = 0.37e$ in MP), which is almost fully recovered at $t = T$ with an integrated charge density of $\bar{Q}_G = 0.48e$. Overall, in EP, approximately half of the hole density oscillates between the ring and the ethyl group, in contrast to P, where less than 10% of the hole density undergoes relocation. To compare the donating effect of the two alkyl groups on the pyrrole ring, we plot the difference between the $\bar{Q}_P$ values at a given phase of the oscillation; that is, $\Delta\bar{Q}_P^{[AP]}(\varphi_{CM}) = \bar{Q}_P^{[AP]}(\varphi_{CM}) - \bar{Q}_P^{[P]}(\varphi_{CM})$ against φ_{CM}. This plot is shown in Fig. 4(d). However, we emphasize that φ_{CM} is determined by the molecule-specific T characteristic time, and the same φ_{CM} values represent different elapsed time from the ionization. We can observe that the charge donated by the alkyl group leads to about 40% and 23% decrease in the hole density in EP and MP compared to P, respectively. The oscillating feature in MP (see red curves in Fig. 4(d)) shows that due to the length of the alkyl chain, the charge is not efficiently donated to the pyrrole ring. This could be an important reason for the fewer dissociation channels in MP compared to P after photoionization.[13,56,57] In the case of EP, we see similar charge oscillation between P and the ethyl group as between P and the H (see bottom subplots of Fig. 4(a) and (c)). This efficient charge transfer and high degree of charge separation between the two groups (ethyl and pyrrole groups) can lead to clean dissociation at the N–C bond. Moreover, when such molecules are incorporated into 2D materials, like graphene or intercalated graphene,[58,59] the resulting molecular engineering of these materials could further modulate the charge migration and separation dynamics, potentially leading to different nature of charge transfer and dissociation processes. However, further theoretical and experimental investigations would need to be done to confirm this effect.

4 Conclusion

We have analyzed the effect of alkyl donor groups on the correlation driven charge migration in pyrrole derivatives. The ionization potential is redshifted in MP and EP as compared to ionization potential of P. The ionization spectra for all the three cases show a distinct separation (>3 eV) between the states stemming from ionization of molecular orbitals with charge distribution on π-conjugation with adjacent π-bonds and lone pairs. The lone pair electrons on the nitrogen are in the p-orbital and the participation of this lone pair in the π-conjugation can be identified through the ionization spectra. Here we see a large energy difference between the cationic states with and without the contribution of the nitrogen lone pair in π-conjugation. This energy difference is an evidence for the stability of π-conjugation involving the nitrogen lone pairs.

The charge migration dynamics in P show the oscillation of charge between the pyrrole ring and the hydrogen atoms. These types of charge oscillations can be helpful in understanding the fragmentation channels reported in the literature. The charge migration in the three systems shows an increase in the oscillation period which along with the redshift in the ionization potential might be an indicator for the effect of the donor group. In MP, we see the oscillation of charges between the methyl and the pyrrole ring. However, the charge oscillation is more complex and involves more than one period in comparison to that in EP. The hole density on the pyrrole ring with and without the alkyl substituent is also different. We observed that the methyl leads to 23% increase in the hole density, whereas it is about 40% for EP. This might be explained by the effect of electron donating and withdrawing groups.

We have also explored the effect of alkyl substitution in pyrrole on the N-atom. In several drugs and biomolecules, the substituents are also found to be on the 2nd/5th or the 3rd/4th positions in the pyrrole ring (counting counterclockwise from the N atom). Similar investigation of the pyrrole derivatives on these positions will give more information related to the type of substituents accepted by pyrrole, the effect of electronegativity of nitrogen and the substituents in the charge migration dynamics. It would also give additional insight into the effective charge transfer from the alkyl substituents to the pyrrole group. Furthermore, such an investigation would improve our understanding on how the substituent's position and the site (such as nitrogen or carbon) influence both the timescale required for similar charge migration between the alkyl group and the pyrrole ring, and how long the charge remains localized on the pyrrole ring. This type of information is key to materials design and understanding of the photosensitive biomolecules in nature, for example for detailed understanding of the molecular structure of porphyrins. The calculated pure electronic charge migration dynamics can be experimentally measured using a pump–probe setup similar to the one reported by F. Calegari *et al.*,[28] or time and angle-resolved photoelectron momentum spectroscopy as reported by K. Baumgartner *et al.*[60] Additionally, core hole clock spectroscopy can also be used to measure electron-charge lifetimes down to the attosecond scale as reported by H. Marroux *et al.*[61,62]

Author contributions

Conceptualization: G. N., K. C., and M. U. K. Investigation: A. I. K., G. N., K. C., and M. U. K. Methodology: A. I. K., G. N., K. C.,

M. U. K., and V. D. Project administration: M. U. K. Software: A. I. K., G. N., M. U. K., and V. D. Resources: G. N. and M. U. K Supervision: M. U. K. Validation: A. I. K., K. C., M. U. K., and V. D. Visualization: G. N., M. U. K., and K. C. Writing – original draft: A. I. K., G. N., K. C., M. U. K., and V. D. Writing – review & editing: A. I. K., G. N., K. C., M. U. K., and V. D.

Conflicts of interest

There are no conflicts to declare.

Data availability

The datasets used and/or analysed during the current study are available from the corresponding author on reasonable request.

Acknowledgements

The ELI ALPS project (GINOP-2.3.6-15-2015-00001) is supported by the European Union and it is co-financed by the European Regional Development Fund. This research has also been supported by the IMPULSE project which receives funding from the European Union Framework Programme for Research and Innovation Horizon 2020 under grant agreement no. 871161. GN and MUK also acknowledge project no. 2019-2.1.13-TÉT-IN-2020-00059, which has been implemented with support provided by the National Research, Development and Innovation Fund of Hungary, and financed under the 2019-2.1.13-TÉT-IN funding scheme. AIK and VD acknowledge financial support from the ANR-DFG project FAUST. KC acknowledges funding from the Cluster of Excellence 'CUI: Advanced Imaging of Matter' of the Deutsche Forschungsgemeinschaft (DFG) – EXC 2056 – project ID 390715994.

Notes and references

1 J. Gros, V. Lavigne, F. Thibaud, M. Gammacurta, V. Moine, D. Dubourdieu, P. Darriet and A. Marchal, *J. Agric. Food Chem.*, 2017, **65**, 1058–1069.
2 M. C. Mahmud, R. Keast, M. Mohebbi and R. A. Shellie, *J. Food Sci.*, 2022, **87**, 982–997.
3 C. A. Downes and S. C. Marinescu, *ChemSusChem*, 2017, **10**, 4374–4392.
4 S. Lin, C. S. Diercks, Y.-B. Zhang, N. Kornienko, E. M. Nichols, Y. Zhao, A. R. Paris, D. Kim, P. Yang, O. M. Yaghi and C. J. Chang, *Science*, 2015, **349**, 1208–1213.
5 Y. Fu, X. Cheng, J. Zhao, T. Kong, C. Cui and X. Zhang, *Polym. J.*, 2012, **44**, 1048–1055.
6 T. Y. Chu, J. Lu, S. Beaupré, Y. Zhang, J. R. Pouliot, S. Wakim, J. Zhou, M. Leclerc, Z. Li, J. Ding and Y. Tao, *J. Am. Chem. Soc.*, 2011, **133**, 4250–4253.
7 M. Il'ina, O. Il'in, O. Osotova, S. Khubezhov, N. Rudyk, I. Pankov, A. Fedotov and O. Ageev, *Carbon*, 2022, **190**, 348–358.
8 M. U. Kahaly, *J. Appl. Phys.*, 2009, **105**, 024312.
9 K. Hübler, U. Hübler, W. R. Roper and L. J. Wright, *J. Organomet. Chem.*, 1996, **526**, 199–202.
10 H. Lee, H. Yang and J. Kwak, *Electrochem. Commun.*, 2002, **4**, 128–133.
11 M. M. Salamone, F. Silvestri, M. Sassi, C. M. Mari, R. Ruffo, L. Beverina and G. A. Pagani, *Sol. Energy Mater. Sol. Cells*, 2012, **99**, 101–108.
12 Manju, M. Jain, S. Madas, P. Vashishtha, P. Rajput, G. Gupta, M. U. Kahaly, K. Özdogan, A. Vij and A. Thakur, *Sci. Rep.*, 2020, **10**, 17364.
13 D. A. Blank, S. W. North and Y. T. Lee, *Chem. Phys.*, 1994, **187**, 35–47.
14 K. Grygoryeva, J. Rakovský, I. S. Vinklárek, O. Votava, M. Fárník and V. Poterya, *AIP Adv.*, 2019, **9**, 035151.
15 D. V. Makhov, S. Adeyemi, M. Cowperthwaite and D. V. Shalashilin, *J. Phys. Commun.*, 2022, **6**, 025001.
16 G. Wu, S. P. Neville, O. Schalk, T. Sekikawa, M. N. R. Ashfold, G. A. Worth and A. Stolow, *J. Chem. Phys.*, 2015, **142**, 074302.
17 G. M. Roberts, C. A. Williams, H. Yu, A. S. Chatterley, J. D. Young, S. Ullrich and V. G. Stavros, *Faraday Discuss.*, 2013, **163**, 95–116.
18 L. Blancafort, V. Ovejas, R. Montero, M. Fernández-Fernández and A. Longarte, *J. Phys. Chem. Lett.*, 2016, **7**, 1231–1237.
19 L. S. Cederbaum and J. Zobeley, *Chem. Phys. Lett.*, 1999, **307**, 205–210.
20 A. I. Kuleff and L. S. Cederbaum, *J. Phys. B: At., Mol. Opt. Phys.*, 2014, **47**, 124002.
21 A. I. Kuleff, S. Lünnemann and L. S. Cederbaum, *J. Phys. Chem. A*, 2010, **114**, 8676–8679.
22 V. Despré, A. Marciniak, V. Loriot, M. C. E. Galbraith, A. Rouzée, M. J. J. Vrakking, F. Lépine and A. I. Kuleff, *J. Phys. Chem. Lett.*, 2015, **6**, 426–431.
23 K. Chordiya, V. Despré, B. Nagyillés, F. Zeller, Z. Diveki, A. I. Kuleff and M. U. Kahaly, *Phys. Chem. Chem. Phys.*, 2023, **25**, 4472–4480.
24 M. Lara-Astiaso, D. Ayuso, I. Tavernelli, P. Decleva, A. Palacios and F. Martín, *Faraday Discuss.*, 2016, **194**, 41–59.
25 M. Vacher, M. J. Bearpark, M. A. Robb and J. P. Malhado, *Phys. Rev. Lett.*, 2017, **118**, 083001.
26 K.-J. Yuan and A. D. Bandrauk, *J. Phys. Chem. A*, 2019, **123**, 1328–1336.
27 D. Haase, G. Hermann, J. Manz, V. Pohl and J. C. Tremblay, *Symmetry*, 2021, **13**, 205.
28 F. Calegari, D. Ayuso, A. Trabattoni, L. Belshaw, S. De Camillis, S. Anumula, F. Frassetto, L. Poletto, A. Palacios and P. Decleva, *et al.*, *Science*, 2014, **346**, 336–339.
29 E. P. Månsson, S. Latini, F. Covito, V. Wanie, M. Galli, E. Perfetto, G. Stefanucci, H. Hübener, U. De Giovannini and M. C. Castrovilli, *et al.*, *Commun. Chem.*, 2021, **4**, 73.
30 V. Despré and A. I. Kuleff, *Phys. Rev. A*, 2022, **106**, L021501.
31 K. Chordiya, V. Despréé, M. U. Kahaly and A. I. Kuleff, *Phys. Rev. A*, 2022, **105**, 062808.

32 V. Despré and A. I. Kuleff, *Theor. Chem. Acc.*, 2019, **138**, 1–6.
33 A. S. Folorunso, A. Bruner, F. Mauger, K. A. Hamer, S. Hernandez, R. R. Jones, L. F. DiMauro, M. B. Gaarde, K. J. Schafer and K. Lopata, *Phys. Rev. Lett.*, 2021, **126**, 133002.
34 F. Mauger, A. S. Folorunso, K. A. Hamer, C. Chandre, M. B. Gaarde, K. Lopata and K. J. Schafer, *Phys. Rev. Res.*, 2022, **4**, 013073.
35 E. Belles, F. Rabilloud, A. I. Kuleff and V. Despré, *J. Phys. Chem. A*, 2024, **128**, 163–169.
36 E. S. Kadantsev, R. Klooster, P. L. De Boeij and T. Ziegler, *Mol. Phys.*, 2007, **105**, 2583–2596.
37 G. te Velde, F. M. Bickelhaupt, E. J. Baerends, C. Fonseca Guerra, S. J. A. van Gisbergen, J. G. Snijders and T. Ziegler, *J. Comput. Chem.*, 2001, **22**, 931–967.
38 E. J. Baerends, T. Ziegler, A. J. Atkins, J. Autschbach, O. Baseggio, D. Bashford, A. Bérces, F. M. Bickelhaupt, C. Bo, P. M. Boerrigter, C. Cappelli, L. Cavallo, C. Daul, D. P. Chong, D. V. Chulhai, L. Deng, R. M. Dickson, J. M. Dieterich, F. Egidi, D. E. Ellis, M. van Faassen, L. Fan, T. H. Fischer, A. Förster, C. Fonseca Guerra, M. Franchini, A. Ghysels, A. Giammona, S. J. A. van Gisbergen, A. Goez, A. W. Götz, J. A. Groeneveld, O. V. Gritsenko, M. Grüning, S. Gusarov, F. E. Harris, P. van den Hoek, Z. Hu, C. R. Jacob, H. Jacobsen, L. Jensen, L. Joubert, J. W. Kaminski, G. van Kessel, C. König, F. Kootstra, A. Kovalenko, M. V. Krykunov, P. Lafiosca, E. van Lenthe, D. A. McCormack, M. Medves, A. Michalak, M. Mitoraj, S. M. Morton, J. Neugebauer, V. P. Nicu, L. Noodleman, V. P. Osinga, S. Patchkovskii, M. Pavanello, C. A. Peeples, P. H. T. Philipsen, D. Post, C. C. Pye, H. Ramanantoanina, P. Ramos, W. Ravenek, M. Reimann, J. I. Rodríguez, P. Ros, R. Rüger, P. R. T. Schipper, D. Schlüns, H. van Schoot, G. Schreckenbach, J. S. Seldenthuis, M. Seth, J. G. Snijders, M. Solà, M. Stener, M. Swart, D. Swerhone, V. Tognetti, G. te Velde, P. Vernooijs, L. Versluis, L. Visscher, O. Visser, F. Wang, T. A. Wesolowski, E. M. van Wezenbeek, G. Wiesenekker, S. K. Wolff, T. K. Woo and A. L. Yakovlev, *Adf 2022.103, Scm*, 2022.
39 G. te Velde and E. J. Baerends, *Phys. Rev. B: Condens. Matter Mater. Phys.*, 1991, **44**, 7888–7903.
40 E. Van Lenthe and E. J. Baerends, *J. Comput. Chem.*, 2003, **24**, 1142–1156.
41 J. P. Perdew, K. Burke and M. Ernzerhof, *Phys. Rev. Lett.*, 1996, **77**, 3865–3868.
42 T. Pilati and A. Forni, *J. Appl. Crystallogr.*, 1998, **31**, 503–504.
43 J. Breidbach and L. S. Cederbaum, *J. Chem. Phys.*, 2003, **118**, 3983–3996.
44 G. Angonoa, O. Walter and J. Schirmer, *J. Chem. Phys.*, 1987, **87**, 6789–6801.
45 C. Leforestier, R. H. Bisseling, C. Cerjan, M. D. Feit, R. Friesner, A. Guldberg, A. Hammerich, G. Jolicard, W. Karrlein, H.-D. Meyer, N. Lipkin, O. Roncero and R. Kosloff, *J. Comput. Phys.*, 1991, **94**, 59–80.
46 A. I. Kuleff, J. Breidbach and L. S. Cederbaum, *J. Chem. Phys.*, 2005, **123**, 044111.
47 A. I. Kuleff, *Attosecond Molecular Dynamics*, The Royal Society of Chemistry, 2018, ch. 4, pp. 103–138.
48 A. J. van den Brom, M. Kapelios, T. N. Kitsopoulos, N. H. Nahler, B. Cronin and M. N. Ashfold, *Phys. Chem. Chem. Phys.*, 2005, **7**, 892–899.
49 C. D. Cooper, A. D. Williamson, J. C. Miller and R. N. Compton, *J. Chem. Phys.*, 1980, **73**, 1527–1537.
50 G. F. Crable and G. L. Kearns, *J. Phys. Chem.*, 1962, **66**, 436–439.
51 G. I. Cárdenas-Jirón, C. Venegas, R. López and M. I. Menéndez, *J. Phys. Chem. A*, 2008, **112**, 8100–8106.
52 A. I. Kuleff, S. Lünnemann and L. S. Cederbaum, *Chem. Phys.*, 2012, **399**, 245–251.
53 L. S. Cederbaum, W. Domcke, J. Schirmer and W. von Niessen, *Adv. Chem. Phys.*, 1986, 115–159.
54 M. S. Deleuze and L. S. Cederbaum, *Phys. Rev. B: Condens. Matter Mater. Phys.*, 1996, **53**, 13326.
55 M. Hervé, V. Despré, P. Castellanos Nash, V. Loriot, A. Boyer, A. Scognamiglio, G. Karras, R. Brédy, E. Constant and A. G. G. M. Tielens, *et al.*, *Nat. Phys.*, 2021, **17**, 327–331.
56 G. Tourillon, S. Raaen, T. A. Skotheim, M. Sagurton, R. Garrett and G. P. Williams, *Surf. Sci.*, 1987, **184**, L345–L354.
57 C.-M. Tseng, Y. T. Lee and C.-K. Ni, *J. Phys. Chem. A*, 2009, **113**, 3881–3885.
58 T. P. Kaloni, M. Upadhyay Kahaly, Y. C. Cheng and U. Schwingenschlögl, *EPL*, 2012, **99**, 57002.
59 S. Madas, S. K. Mishra, S. Kahaly and M. U. Kahaly, *Sci. Rep.*, 2019, **9**, 10307.
60 K. Baumgärtner, M. Reuner, C. Metzger, D. Kutnyakhov, M. Heber, F. Pressacco, C.-H. Min, T. R. Peixoto, M. Reiser and C. Kim, *et al.*, *Nat. Commun.*, 2022, **13**, 2741.
61 H. J. Marroux, A. P. Fidler, A. Ghosh, Y. Kobayashi, K. Gokhberg, A. I. Kuleff, S. R. Leone and D. M. Neumark, *Nat. Commun.*, 2020, **11**, 5810.
62 F. E. Oropeza, M. Barawi, E. Alfonso-González, J. F. Trigo, C. Guillén, F. Saiz and I. J. Villar-Garcia, *et al.*, *J. Mater. Chem. C*, 2021, **9**, 11859–11872.